PROCEEDINGS OF SPIE

SPIEDigitalLibrary.org/conference-proceedings-of-spie

Cohen class time-frequency mapping in the analysis of the non-stationary parameters of a wave gaussian beam at the atmospheric path output

T. I. Arsenyan, E. A. Babanin, A. V. Blank, R. F. Stryungis, N. A. Suhareva

T. I. Arsenyan, E. A. Babanin, A. V. Blank, R. F. Stryungis, N. A. Suhareva, "Cohen class time-frequency mapping in the analysis of the non-stationary parameters of a wave gaussian beam at the atmospheric path output," Proc. SPIE 10833, 24th International Symposium on Atmospheric and Ocean Optics: Atmospheric Physics, 108332Q (13 December 2018); doi: 10.1117/12.2504659

SPIE.

Event: XXIV International Symposium, Atmospheric and Ocean Optics, Atmospheric Physics, 2018, Tomsk, Russian Federation

Cohen class time-frequency mapping in the analysis of the non-stationary parameters of a wave gaussian beam at the atmospheric path output

T. I. Arsenyan[1], E. A. Babanin[1], A. V. Blank[1,2], R. F. Stryungis[1], and N. A. Suhareva[1]

[1]Moscow State M.V. Lomonosov University, Physics Faculty, Russia, 119991, Moscow, Leninskie Gory 1-2

[2]S.P Korolev Rocket and Space Corporation "Energia", Russia, 141070, Korolev, Moscow area, Lenina street 4a

ABSTRACT

The experimental results of the time-frequency maps structure research are presented. The maps were received on the basis of Cohen class square mapping, particularly, using Wigner-Ville pseudo-distribution. Quasi synchronous monitoring of the atmospheric channel conditions and of a beam intensity spatial distribution is realized by means of the high-speed cameras of computer vision. The cameras record dynamics of a profile intensity distribution of a single-mode collimated signal beam at the receiving plane and that of the reflected sounding multimode beam. At an input of the long distance atmospheric path there comes the generalized Gaussian signal beam with the defined Rayleigh length and wavefront curvature. At the path output the spatial moments of the beam from the zero to the fourth orders are registered. The spatial moments allow to describe in details beam distortions along the propagation path with the temporary resolution not less than 1 ms.

Keywords: free space optical channel, turbulence, non-linear time-frequency mapping, generalized Gaussian beam, the central spatial moments.

PACS: 42.25.Dd, 42.68.Bz.

Introduction

The intensity distribution of the sounding or signal wave beam refractive modulation are the nonstationary and statistically nonuniform processes. They can be considered as the sources of the additive and multiplicative hindrances disturbance. The type of operating signal-code sequences depends on the number of parameters such as the type of the used spatial signal-coding structures, the number of the involved subchannels during the work with beams multiplets, basic code radiation characteristics (the polarization, the orbital moment, the beam profile or its intensity) and affects the disturbances parameters set. However, for any set of parameters the dynamic range and spatio-temporal structure of the disturbances have to be the key characteristic registered in a frequency range from the highest frequency of a signal sampling to the frequency of the informational frames.

1. FLUCTUATIONS OF CHANNEL AND SIGNAL PARAMETERS

Free space optical communication channels are used in laser location and navigation systems, laser remote sensing systems, the systems of laser targeting and mobile laser communication.[1] For optical band atmospheric transmission channels represent the channels with the randomly non-uniform parameters.[2] The propagation conditions in such channels have significant effect on the system range, the transfer, reception and information processing efficiency. Optical channels with scattering are usually described using the concept of meteorological visibility range.

The signal distribution along the open path is defined by value of the refraction index. For the tropospheric paths it is approximately estimated by the ratio:

Further author information: (Send correspondence to A. V. Blank)
A. V. Blank : E-mail: BlankArkadiy@physics.msu.ru

24th International Symposium on Atmospheric and Ocean Optics: Atmospheric Physics, edited by Gennadii G. Matvienko, Oleg A. Romanovskii, Proc. of SPIE Vol. 10833, 108332Q
© 2018 SPIE · CCC code: 0277-786X/18/$18 · doi: 10.1117/12.2504659

$$n-1=77.6\left(1+7.52*\lambda^{-2}10^{-3}\right)\frac{P}{T}10^{-6} \quad (1)$$

Here T is an absolute temperature. P is a pressure in millibars. λ is a wavelength in micrometers. Radiation propagating through the turbulent atmosphere experiences, besides the power losses, a casual energy redistribution bound to the presence of effects of the amplitude and phase fluctuations takes place.[3] These fluctuations are generated by random spatio-temporal changes of the refraction index of the medium along all the way of beam propagation.[4] Observed variations of the refraction index are mostly caused by temperature fluctuations. It is possible to define the fluctuations structure of the refraction index, thus, estimating the temperature fluctuations. In an assumption of the locally homogeneous and isotropic turbulence A.N. Kolmogorov received the so-called law of "two thirds"for the field of velocities fluctuations. A.M. Obukhov extended it to fluctuations of meteo parameters. As a result, the expression describing the law of two thirds for fluctuations of the refraction index was obtained:

$$D_n(l)=C_n^2 l^{2/3} \quad (2)$$

here $D_n(l)$ is a structural function of the refraction index fluctuations which is an average square of the value difference in two points separated at the distance l. C_n^2 is a structural characteristic of the refraction index fluctuations.

The "two thirds" law is fair for an inertial interval. There is no energy accumulation in eddies of any size, everything is defined by inertial forces. In the breaking up process eddies become more and more smaller. As a result of a friction their energy begins to turn into heat, so, we pass into dissipation area. The law was derived on the assumption of local uniformity and isotropy of the medium. In classical representation the quasistationary systems and processes are considered. However the distinctive characteristic of the near-the-ground atmosphere is its inhomogeneity and non-stationarity. Fluctuations describe the random changes of the received signal parameters caused by the composite nature of propagation and random spatio-temporal changes of the channel parameters. Coherent optical radiation propagating through the atmosphere experiences the random fluctuations.[5] Inherently they can be specified as follows:

- the deviation of an arrival angle from the optical axis direction of a transmitting receiving system leading to a random drift of a beam cross-section at the detecting plane. That is bound to space gradients of an optical density;
- the beam cross section fluctuations at the receiving plane (so called "respiration") at the expense of the efficient curvature variations of an optical density spatial distribution along the path;
- the beam rotational fluctuations are significant for multigaussian beams propagation. They arise at hit of vortex currents in the aspect angle of the beam.

The beam interaction with propagation medium is defined by the ratio of the beam diameter and inhomogeneities scale.[6] If this relation is small, one can expect that the main effect of the inhomogeneities influence will affect as a refractive type phenomenon. That leads to random deviations of the beam center from average location. It follows that in case of an isotropic turbulence the beam center shift must conform with the Rayleigh distribution law.

If the beam diameter is approximately equal to the inhomogeneities scale , the effect of inhomogeneities is similar to that of the lenses. The beam spreading in this cases will be small, and the expected fluctuations will not be considerable. If the relation of the beam diameter to the inhomogeneities scale is large, locally limited parts of the beam will undergo the independent processes of diffraction and scattering. Therefore for the long distance paths the strong fluctuations are typical.

The description of fluctuations requires that the main attention should be paid to the characteristic frequency, modulation depth and porosity time ratio. The second and the third characteristics are in details described in various models, but the range of the characteristic frequencies is investigated rather poorly. In this work one of the acceptable methods for the analysis of the non-stationary ranges of the beam positional parameter variations at the atmospheric path output is presented.

2. NON-LINEAR TIME-FREQUENCY MAPPINGS

The contemporary optical problems are misaligned in the area of generation, filtering, analysis of the pulses of different width and modulation types detected at the threshold of the time and energetic characteristics of the radiation source and the recorders. The traditional spectral decomposition of signals is based on an assumption of a quasistationarity of the process considering and uses the infinite on duration and extremely narrow-band harmonic components as the basic functions. The real physical signal of the given energy has to be limited in time, therefore information on its spectrum has to contain a temporary variable at least indirectly. Mathematical statement of a time-frequency problem analysis assumes integral mapping of the recorded signal with the subsequent introduction of additional physical properties such as capacity, energy, length, coherence radius and other characteristics inherent in concrete signal types.[7,8] Physically significant parameters of a signal are usually consisted in its quadratic forms (capacity, energy). Therefore for a signal influence or an excitation level of a generating system estimation it is necessary to use the apparatus of time-frequency description of the signal energy properties. The energetic time-frequency distribution of a signal is initially drawn up on the basis of quadratic forms both for the frequency and time analysis.[9,10] Irrespective of the representation type of the considered signal its total energy should not change, therefore for any types of bases the ratio has to be satisfied:

$$E_s = \int_{-\infty}^{\infty} |s(t)|^2 \, dt \equiv \int_{-\infty}^{\infty} |S(\omega)|^2 \, d\omega \tag{3}$$

Integrands in (3) can be interpreted as the signal energy density at present time or at given frequency. Lets define one more detailed energy characteristic of a signal $s(t)$representing the joint time-frequency distribution $\epsilon_s(t,\omega)$ described by an energy density function and satisfying the common integral ratio:

$$E_s = \int_{-\infty}^{\infty} \int_{-\infty}^{\infty} \epsilon_s(t,\omega) \, dt d\omega \tag{4}$$

and two marginal properties:

$$\begin{aligned} \int_{-\infty}^{\infty} \epsilon_s(t,\omega) \, dt &= |S(\omega)|^2 \\ \int_{-\infty}^{\infty} \epsilon_s(t,\omega) d\omega &= |s(t)|^2 \end{aligned} \tag{5}$$

The ratios presented (4) and (5) are consistent mathematically, but are unsuitable for the conjugate variables which measurement accuracy is limited to an indeterminacy principle:

$$\sigma_t \sigma_\omega \geqslant \frac{1}{2}. \tag{6}$$

To resolve contradiction one can use quasiprobability Wigner-Ville mapping which in some cases can accept the negative value for the signal structures which do not have physical realizations in classical states:[7,11]

$$\begin{aligned} W_s(t,\omega) &= \int_{-\infty}^{\infty} s(t+\tau/2) \cdot s^*(t-\tau/2) e^{-i\omega\tau} d\tau, \\ W_s(t,\omega) &= \int_{-\infty}^{\infty} S(\omega+\phi/2) \cdot S^*(\omega-\phi/2) e^{-i\phi t} d\phi. \end{aligned} \tag{7}$$

here $s(t)$,
$S(\omega)$ is an initial signal and its Fourier transform.

The most significant properties of the considered mapping in this problem are:

- Marginal distributions:

$$\int_{-\infty}^{\infty} W_s(t,\omega)d\omega = |S(\omega)|^2$$
$$\int_{-\infty}^{\infty} W_s(t,\omega)\,dt = |s(t)|^2$$

- Definition on the real axis of values:

$$W_s(t,\omega) \in \mathbb{R}, \quad \forall\ t,\ \omega$$

- Distribution for the filtered signals:

$$y(t) = \int_{-\infty}^{\infty} h(t-s)\cdot x(s)\,ds \ \Rightarrow\ W_y(t,\omega) = \int_{-\infty}^{\infty} W_h(t-s,\omega)\cdot W_x(s,\omega)\,ds$$

- Distribution for the modulated signals:

$$y(t) = m(t)\cdot s(t) \ \Rightarrow\ W_y(t,\omega) = \int_{-\infty}^{\infty} W_m(t,\omega-\phi)\cdot W_x(s,\phi)d\phi$$

- Preservation of a cutoff in the frequency and time ranges:

$$s(t) = 0,\ |t| > T \ \Rightarrow\ W_x(t,\omega) = 0,\ |t| > T$$
$$S(\omega) = 0,\ |\omega| > B \ \Rightarrow\ W_x(t,\omega) = 0,\ |\omega| > B$$

Physical and mathematical validity of the time-frequency Wigner-Ville distribution , the listed above properties of initial distribution and its derivatives makes it a powerful universal method for time-frequency analysis of nonstationary signals[12] . However the results interpretation is very complicated first of all because of the strong interference distortions. As Wigner-Ville distribution is built on the basis of square function from an initial signal, we shall analyze the interference processes in the approximation of a square principle of superposition:

$$W_{s_1+s_2}(t,\omega) = W_1(t,\omega) + W_2(t,\omega) + 2\mathbb{R}\left\{W_{1,2}(t,\omega)\right\} \tag{8}$$

Where

$$W_{1,2}(t,\omega) = \int_{-\infty}^{\infty} s_1(t+\tau/2)s_2^*\,(t-\tau/2)e^{i\omega\tau}d\tau \tag{9}$$

The expression (9) is called Wigner-Ville cross-mapping. The interference components in this distribution are formed between the "original"components of the signal and oscillate in the direction, perpendicular to the line connecting the"originals" centers with the frequency, proportional to distance between the "originals"centers.[7]

The essential problem of data flows processing in real time arising in work with Wigner-Ville distribution is the practical impossibility to execute calculations before the completion of a signal registration. Really, for the integral calculation it is necessary to define value of two-parameter function in the whole time range:

$$q_s(t,\tau) = s(t+\tau/2)\cdot s^*\,(t-\tau/2) \tag{10}$$

If we put up with the finite delay on a time scale of the processed signal concerning the detecting time it is possible to use a sliding window method as it was made in the shortened Fourier mapping and to determine Wigner-Ville pseudo-distribution by the following ratio:

$$PW_s(t,\omega) = \int_{-\infty}^{\infty} h(\tau)\cdot s(t+\tau/2)\cdot s^*\,(t-\tau/2)e^{-i\omega\tau}d\tau \tag{11}$$

here $h(t)$ is a window profile. Pseudo-distribution can be interpreted as a smoothing of the initial distribution by means of the frequency filter according to integral transformation:

$$PW_s(t,\omega) = \int_{-\infty}^{\infty} H(\omega - \phi) \cdot W_s(t,\phi) d\phi, \tag{12}$$

where $H(\omega)$ is a Fourier transform of $h(t)$. As a side effect the window transformation offered allows to get rid of oscillating interference components along the time axis. The reverse side of window transformation is losing of some properties by Wigner-Ville quasi distribution inherent in initial distribution. For instance, for quasi distribution the marginal ratios, the unitarity and the frequency localization are unfair.

3. COHEN CLASS MAPPINGS

Wigner-Ville mapping can not be treated as simultaneous probability distribution of an observed signal in time and frequency because it accepts the negative values. Interpretation of this mapping function as certain auxiliary, satisfying many useful ratios which often pass to marginal probability distributions as the inherited properties is more justified. It should be noted that expression(7) can be presented not only in the bilinear mapping form of the recorded signals. The formula (7) actually doubles the number of the independent variables which are initially used in definition of the initial system dynamic condition. Accordingly Wigner-Ville mapping has twice larger number of degree of freedoms. At rigorous approach to bilinear mapping of an analytical signal it is possible to prove the impossibility of creation of positively definite real mapping. Actually the Wigner function can be considered as the simplest of available bilinear mappings of a wave function.[7,13]

The circumvention of restrictions for simultaneous resolution of temporary and frequency characteristics for a nonstationary refraction process is possible when performing non-linear time-frequency mappings of the Cohen class, covariant in relation to the time and frequency shift.[7] We will define integral signal mapping $s(t)$ or its equidistant time series s_k of Cohen class as follows:

$$C_s(t,\omega;f) = \iiint_{-\infty}^{\infty} e^{-i\phi(l-t)} f(\phi,\tau) s(l+\tau/2) s^*(l-\tau/2) e^{-i\omega\tau} d\phi dl d\tau, \tag{13}$$

here $f(\phi,\tau)$ is a parametrization function. Let us construct a number of the mappings allowing to define dynamic band spectra of the signal choosing the type of parametrization function. As a basic dynamic spectrum let us make use of Wigner-Ville mapping got from (13) at the choice of unit parametrization function:

$$f_{WV}(\phi,\tau) \equiv 1, \quad WV_s(t,\omega) = \iint_{-\infty}^{\infty} s(t+\tau/2) s^*(t-\tau/2) e^{-i\omega\tau} d\phi ds d\tau \tag{14}$$

For an analysis and the cutoff of the interference terms contained in the time- frequency distributions (14), the window transformations in the frequency and temporary ranges are applied allowing to perform the necessary depth smoothing of rapidly oscillating components:

$$SPWV_s(t,\omega) = \int_{-\infty}^{\infty} h(\tau) \int_{-\infty}^{\infty} g(l-t) \cdot s(l+\tau/2) \cdot s^*(l-\tau/2) dl e^{-i\omega\tau} d\tau, \tag{15}$$

here $h(\omega)$ is a frequency window function, $g(t)$ is a time window function. The synthesized dynamic range can be compared with the signal spectrogram. This spectrogram has lower than Wigner-Ville resolution , but it is free from the interference components generated by cross products at square mapping of multicomponent signals. This spectrogram also refers to Cohen class mapping and can be written using the parametrization function which coincides with Wigner-Ville distribution:

$$S_x(t,\omega) = \iint_{-\infty}^{\infty} W_h(l-t,\phi-\omega) W_s(l,\phi) d\phi dl \tag{16}$$

Besides the listed three square integral mappings (7, 15, 16) the Choi-Williams, Margenau-Hill and Born-Jordan mappings can be used for the time-frequency characteristics analysis.

4. OPTICAL SYSTEM FOR SPATIAL WAVE BEAM MOMENTS CONTROL

1350 meters long experimental path passes at the height more than 30 meters over an industrial zone that provides plurality of natural and industrial factors for the refractive index disturbances. The control of initial curvature of a beam wavefront, formation of astigmatic distortions of Gaussian and super-Gaussian beams allows to investigate the dynamic transmitting characteristics of the open space optical path under the conditions of the strong turbulent distortions. The control of a beam wavefront profile at the path input is carried out using the system of confocally located non-spherical lens and parabolic interference mirror. The lens position can be changed along three directions with an accuracy of one micron, that being comparable with a wavelength of the used radiation (1082 nanometers). The recording of the intensity distribution sequences at the output of the atmospheric path is carried out with frequencies from 500 Hz up to 2000 Hz over a square aperture with the linear size 256x256 mm^2. Each frame sequence is considered to be an ensemble of realization of the beam states. For each realization the space moments from the zero order to the fourth one are calculated.

The equivalent optical scheme consists of two lenses with the focal lengths f_1 and f_2. At the distances l_1 from the first lens the strangulation of the energy bearing laser beam. The first lens can move in three orthogonal directions, Z coincides with an optical axis of the simplified scheme l_2 is the distance between the lenses. L is the distance between the second lens and the strangulation . Lets define the properties of the stigmatic Gaussian beams at the input and at the output of the optical system using two parameters, - the strangulation position relative to the lens plane (input or output) and Rayleigh length:

$$z_0^{in} = \frac{k\omega_0^{in\ 2}}{2}, \quad z_0^{out} = \frac{k\omega_0^{out\ 2}}{2}, \tag{17}$$

ω_0^{in}, ω_0^{out} are the sizes of the beam strangulations at the input of two-lens group and at the output of the group . Using the early obtained[14] ratios for input and output positional and configuration parameters of a stigmatic Gaussian beam lets get the dependence for the beam size at the registration plane:

$$\frac{\omega(\Delta)}{\omega_0^{in}} = \sqrt{1 + \left(\frac{L(\Delta) - L_R}{z_0^{out}(\Delta)}\right)^2}, \tag{18}$$

$$L(\Delta) = f_2 \frac{[f_1 l_1 + l_2(f_1 - l_1)]\,[f_2 l_1 - (f_1 - l_1)(f_2 - l_2)] + z_0^{in\ 2}(f_1 - l_2)(f_1 + f_2 - l_2)}{[l_1 f_2 - (f_1 - l_1)(f_2 - l_2)]^2 + z_0^{in\ 2}(f_1 + f_2 - l_2)^2},$$
$$l_1(\Delta) = l_1 - \Delta, \quad l_2(\Delta) = f_1 + f_2 + \Delta,$$

where $L(\Delta)$ and $z_0^{out}(\Delta)$ are the beam strangulation position and its Rayleigh length at the positional lens offset. Transition to the beam grouping zone at the distances of several hundred or thousand meters is possible at rather great values of Rayleigh length of the initial beam.[15,16] For the used value z_0^{in} =125 meters the maximal range of the beam grouping is a little bit more than 2600 meters.

In Fig. 1 the calculated beam radius dependences on the position lens location for various screen positions are presented. The characteristic feature of the dependences obtained is the asymmetry of the right- and the left-hand branches of the rearrangement characteristics. That distinguishes them from conventional rearrangement profiles of cross- section dimensions of a Gaussian beam under its free space propagation.

The experimental tests were carried out at the 1350 meters long atmospheric path under the turbulence development level corresponding to $\beta^2 = 1.3$. The frame frequency was 1 kHz. The recording time was 1 s. The digit capacity of the image is equal to 8 bits and the display scale was 1 pt/mm. The space moments from the first to the fourth orders were analyzed for the step shift of the positional lens equal to 5 μm. The range of the lens shift was about $\pm$ 350 μm and was limited by beam dimension exceeding the registration aperture limits.

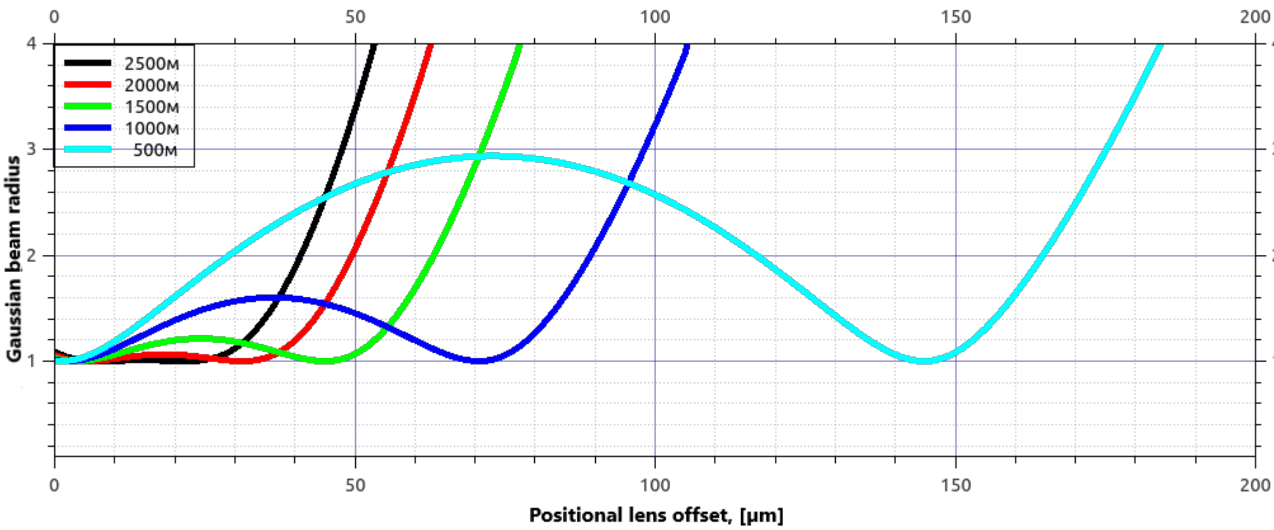

Figure 1. The optical scheme of the beam profile control.

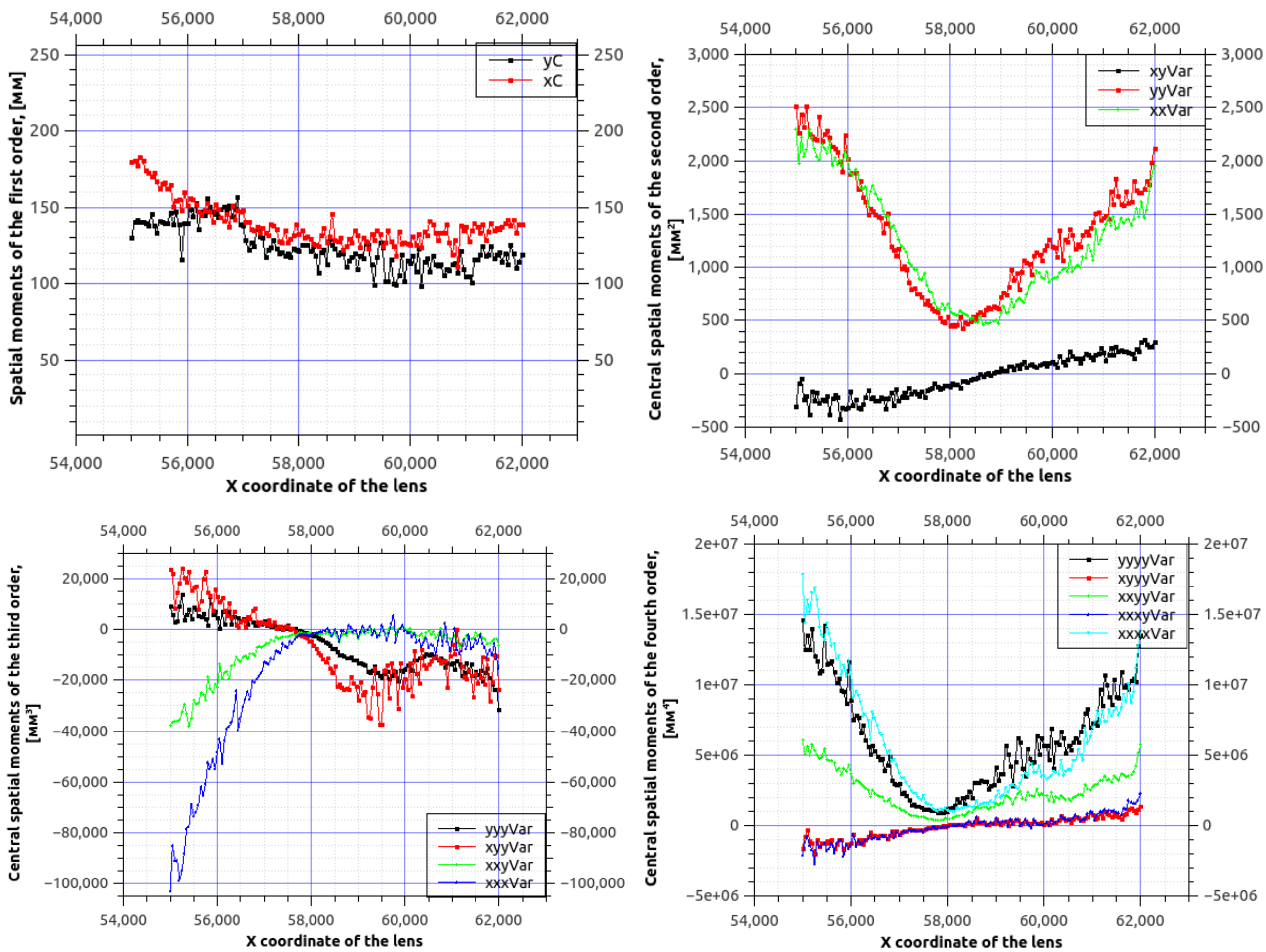

Figure 2. The experimental monitoring of space moments rearrangements for a stigmatic Gaussian beam

The example of the obtained dependences of beam space parameters on the lens location is shown in Fig. 2.

The diagonal elements of the second space moment demonstrate the dependence similar to that obtained for an axial model accurate within the observed shift direction of the positional lens 1. The observed astigmatism (a non-zero non-diagonal component of the second space moment) and the asymmetry of the intensity distribution are partially formed by an optical system. But mainly they are brought in the intensity distribution by the non-uniform and non-isotropic currents at the path output.

5. THE TIME-FREQUENCY MAPPING OF THE EXPERIMENTAL SERIES

The non-linear time-frequency mappings are very exacting to calculating resources when processing large data series. The number of the carried-out operations when determining a spectral density at a single frequency for a time series length N is proportional to N^2. The reference duration of the processed series without taking into account the window restrictions can be tens of thousand counts. The scenarios of high-speed video streams processing was written using Haskell. All of the video streams was received under the 1350 meters long atmospheric path testing.

Lets consider the informational capacity of square time-frequency mappings for time series of the first and second space moments of a wave beam at the registration plane. The refractive modulation over the long distance path is characterized by a non-stationary spectra in a wide frequency range. The main interpretation difficulty for square signal mapping consists in the separation of characteristic and interference components.[17] The efficient method for the interference components suppression is using the window averaging both in time scale, and in frequency scale.[18] Lets consider a time series consisting of 1000 readings of the horizontal projection for the first space moment. The results of such an averaging for different values of the symmetric Gaussian window are presented in Fig.3.

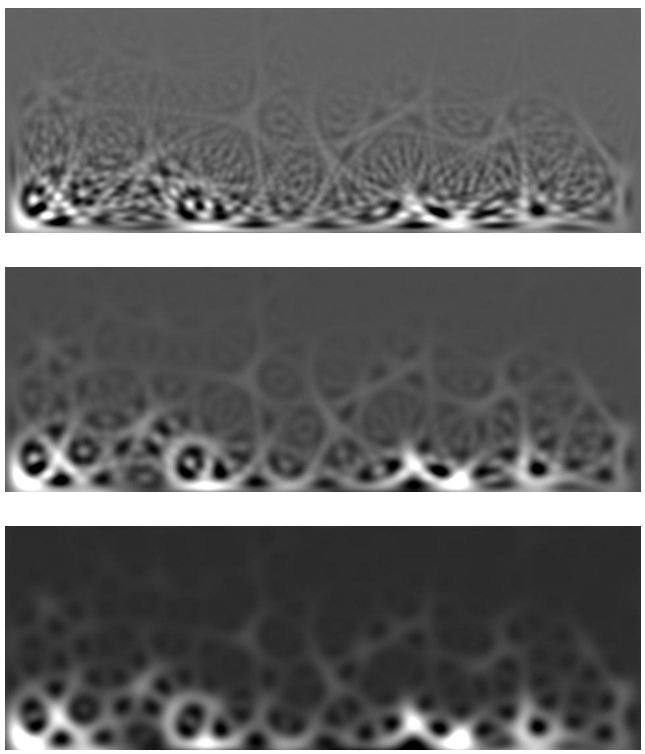

Figure 3. The elimination of the interference components by smoothing. The Gaussian smoothing window increases from top to down and takes 4,7 and 10 discrete steps at time and frequency axes. The frequency scale occupies the range of $[0.0Hz, 312.5Hz]$, the range of the time scale is - $[0.0s, 0.999s]$.

Born-Jordan mapping is one of the most efficient for interference component smoothing and selection of characteristic time-frequency range.[19,20] It refers to Cohen class with symmetrical parametrization function depending on the arguments product:

$$f(\phi,\tau)=\frac{\sin(\pi\phi\tau)}{\pi\phi\tau}. \tag{19}$$

One of the forms of Born-Jordan mapping is:

$$BJ_s(t,\omega)=\int_{-\infty}^{\infty}\frac{1}{|\tau|}\int_{t-\frac{|\tau|}{2}}^{t+\frac{|\tau|}{2}} s\left(l+\frac{\tau}{2}\right)s^*\left(l-\frac{\tau}{2}\right)dle^{-i\omega\tau}d\tau \tag{20}$$

The comparison of Wigner-Ville and Born-Jordan non-linear time-frequency mappings is presented in Fig. 4 for the component of the first space moment of a wave beam which strangulation is behind the registration plane, at the plane and in front of the registration plane. In Fig.2 these positions correspond to positional lens coordinates 56500, 58500 and 60500 shift units.

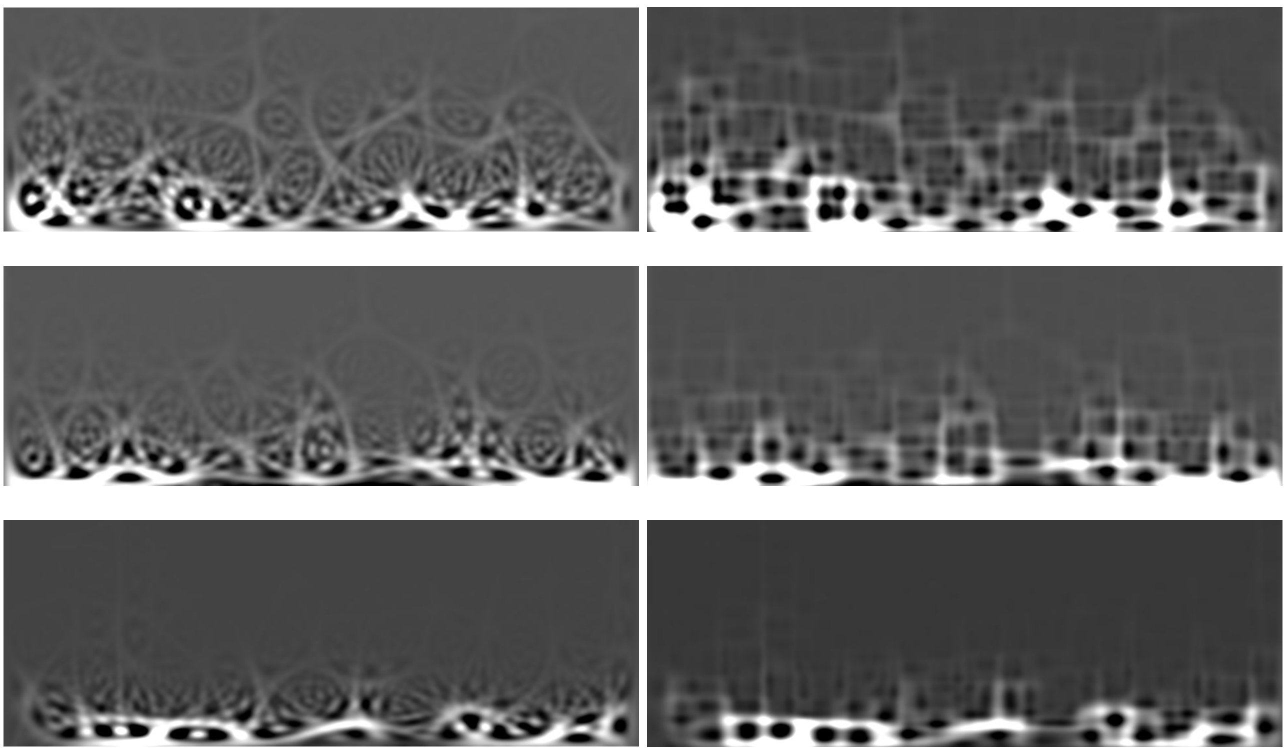

Figure 4. Wigner-Ville mapping (left) and Born-Jordan (right) for a horizontal component of the first space moment of a wave beam. Maps at the top are for a beam with a strangulation in front of the registration plane, in the middle - a strangulation is in the registration plane, below the case of strangulation is behind the registration plane.

The comparison of two mappings of the same process allows to allocate the characteristic process frequencies, the polychromatic impulses duration and to visualize the cascade transformations that are typical for refractive disturbances under the turbulent conditions. The time-frequency maps observed, with the rare exception of the simplest signals like chirp or Gabor atoms, shall not be interpreted directly as the variety of the frequencies combinations realized at the moment. For example, for the pair of time-frequency maps given above Born- Jordan mapping allows to localize pulse influences in the "lattice" points. The symmetrically smoothed Wigner-Ville mapping contains the information about the transitional trajectories between these lattice points and the energy frequency distribution.

The comparative analysis of different types of time-frequency mappings for the same process allows to create a new technique for analysis and interpretation of beam positional characteristics. For example, in Fig. 5 the

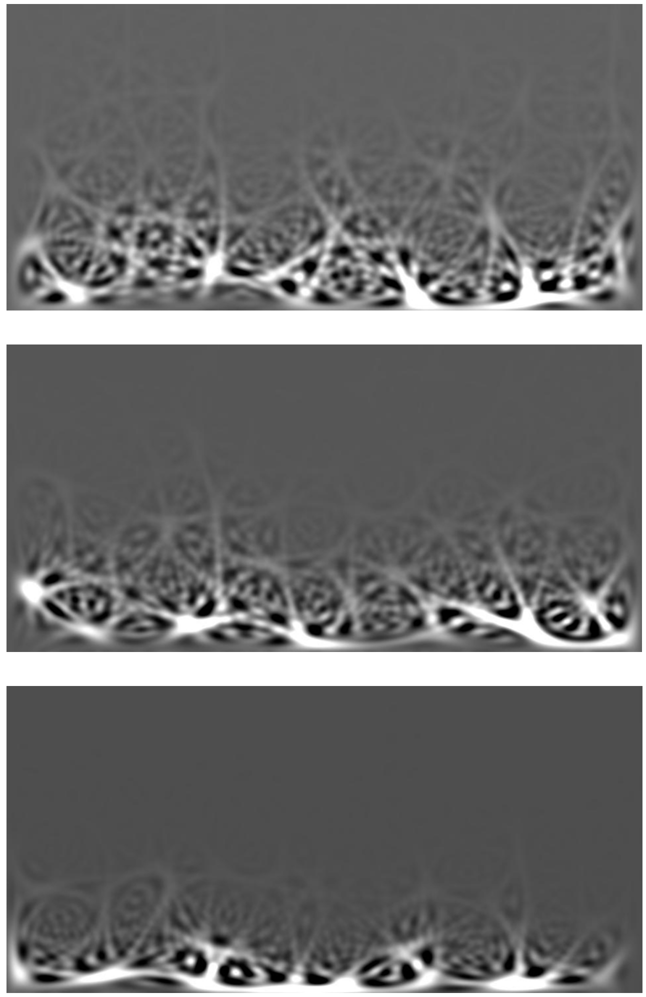

Figure 5. Time-frequency maps for the components of the second space moment: the horizontal diagonal component (at the top), the vertical diagonal component (bottom), the non-diagonal component (in the middle). The frequency diagram occupies the range $[0.0Hz, 499.9Hz]$, the time scale is $[0.0s, 0.999s]$.

mappings for diagonal and non-diagonal components of the second central space moment tensor are presented. These components describe the oscillating and rotational transformations of the intensity profile distribution of the beam.[21] The distinction of the band width in the frequency projection, of the lattice points connectivity on the time-frequency map and the cells geometry manifest the significant anisotropy of refractivity disturbances for the samplings analyzed.

Conclusion

Non-linear time-frequency mappings with various parameterization functions have deep analogies with the quantum mechanics technique allowing to define the mean operator $f(\phi, \tau)$ value for the system at the state with a non-stationary wave function $s(t)$. The basic symmetrically smoothed Wigner-Ville mapping without parametrization function is necessary to treat as the quasi probability time-frequency spectrum corresponding to the process under consideration. The imposing of specially built parametrization functions changes the weight values of non-stationary components of the composite signal and allows to recognize the required process or to define the distinctions of the processes observed.

ACKNOWLEDGMENTS

The work was supported by State Theme "Wave Beams and Pulses in the Nonuniform and Stratified Media" AAAA-A17-117121890022-8.

REFERENCES

[1] Bataille, P., *Analysis of the behavior of a telecommunications system operated optical 0.83 microns in the lower atmosphere*, PhD thesis, Ph. D thesis, University of Rennes, France (1992).

[2] Korotkova, O., [*Random light beams: theory and applications*], CRC press (2013).

[3] Tatarskii, V. I., [*Theory of Fluctuating Phenomena in the Propagation of Waves in a Turbulent Atmosphere*], Office of Technical Services, US Department of Commerce (1960).

[4] Andrews, L. C. and Phillips, R. L., [*Laser beam propagation through random media*], vol. 152, SPIE press Bellingham, WA (2005).

[5] Andrews, L. C., Phillips, R. L., Hopen, C. Y., and Al-Habash, M., "Theory of optical scintillation," *JOSA A* **16**(6), 1417–1429 (1999).

[6] Babanin, E., Kapranov, V., Suhareva, N., Tugaenko, V., and Vohnik, O., "Space-temporal stochastic characteristics of complex amplitude for the sounding vector optical beam," in [*Progress In Electromagnetics Research Symposium-Spring (PIERS), 2017*], 902–908, IEEE (2017).

[7] Cohen, L., [*Time-frequency Analysis*], Electrical engineering signal processing, Prentice Hall PTR.

[8] Hillery, M., O'Connell, R., Scully, M., and Wigner, E., "Distribution functions in physics: Fundamentals," *Physics Reports* **106**(3), 121 – 167 (1984).

[9] Papandreou-Suppappola, A., [*Applications in time-frequency signal processing*], vol. 10, CRC press (2002).

[10] Boashash, B., [*Time-frequency signal analysis and processing: a comprehensive reference*], Academic Press (2015).

[11] Cordero, E. and Nicola, F., "Sharp integral bounds for wigner distributions," *International Mathematics Research Notices* , rnw250 (2016).

[12] Martin, W. and Flandrin, P., "Wigner-ville spectral analysis of nonstationary processes," *IEEE Transactions on Acoustics, Speech, and Signal Processing* **33**(6), 1461–1470 (1985).

[13] Carles, R., Kammerer, C. F., Mauser, N., and Stimming, H. P., "On the time evolution of wigner measures for schrodinger equations," *arXiv preprint arXiv:0803.0667* (2008).

[14] Babanin, E. A., Suhareva, N. A., Vokhnik, O. M., Kapranov, V. V., Matsak, I. S., and Tugaenko, V. J., "Positional characteristics of generalized decentered elliptical gaussian beams on extended atmospheric paths," *Proceedings 2017 Days on Diffraction (DD)* , 24–30 (2017).

[15] Gerrard, A. and Burch, J. M., [*Introduction to matrix methods in optics*], Courier Corporation (1975).

[16] Abramochkin, E. and Volostnikov, V., "Modern optics of gaussian beams," *FizMatLit, Moscow* (2010).

[17] Arsenyan, T., Babanin, E., Kapranov, V., Stryungis, R., Suhareva, N., and Tugaenko, V., "Time-frequency mapping of the positional characteristics of single-and multimode wave beam at the lengthy atmospheric path output," in [*EPJ Web of Conferences*], **161**, 02003, EDP Sciences (2017).

[18] Cordero, E., de Gosson, M., Drfler, M., and Nicola, F., "On the symplectic covariance and interferences of time-frequency distributions," *SIAM Journal on Mathematical Analysis* **50**(2), 2178–2193 (2018).

[19] Cordero, E., de Gosson, M., and Nicola, F., "Time-frequency analysis of born–jordan pseudodifferential operators," *Journal of Functional Analysis* **272**(2), 577–598 (2017).
[20] Cordero, E., de Gosson, M., and Nicola, F., "On the reduction of the interferences in the bornjordan distribution," *Applied and Computational Harmonic Analysis* **44**(2), 230 – 245 (2018).
[21] Goodman, J. W., [*Statistical optics*], John Wiley & Sons (2015).